ACS Photonics

Article

pubs.acs.org/journal/apchd5

Time-Gated DNA Photonic Wires with Förster Resonance Energy Transfer Cascades Initiated by a Luminescent Terbium Donor

Melissa Massey,[†] Mario G. Ancona,[‡] Igor L. Medintz,[§] and W. Russ Algar*,[†]

[†]Department of Chemistry, University of British Columbia, 2036 Main Mall, Vancouver, British Columbia, V6T 1Z1, Canada

[‡]Electronic Science and Technology Division, Code 6876, and [§]Center for Bio/Molecular Science and Engineering, Code 6900, U.S. Naval Research Laboratory, 4555 Overlook Avenue SW, Washington, D.C. 20375, United States

Supporting Information

ABSTRACT: Functional DNA nanotechnology is a rapidly growing area of research with many prospective photonic applications, including roles as wires and switches, logic operators, and smart biological probes and delivery vectors. Photonic wire constructs are one such example and comprise a Förster resonance energy transfer (FRET) cascade between fluorescent dyes arranged periodically along a DNA scaffold. To date, the majority of research on photonic wires has focused on setting new benchmarks for efficient energy transfer over more steps and across longer distances, using almost exclusively organic fluorescent dyes and strictly DNA structures. Here, we expand the range of materials utilized with DNA photonic wires by demonstrating the use of a luminescent terbium complex (Tb) as an initial donor for a four-step FRET cascade along a ∼15 nm long DNA/locked nucleic acid (LNA) photonic wire. The inclusion of LNA nucleotides increases the thermal stability of the photonic wires while the Tb affords time-gated emission measurements and other optical benefits. Time-gating minimizes unwanted background emission, whether from direct excitation of fluorescent dyes along the length of the photonic wire, from excess dye-labeled DNA strands in the sample, or from a biological sample matrix. Observed efficiencies for Tb-to-dye energy transfer are also closer to the predicted values than those for dye-to-dye energy transfer, and the Tb can be used as an initial FRET donor for a variety of next-in-line acceptors at different spectral positions. We show that the key to using the Tb as an effective initial donor is to optimally position the next-in-line acceptor dye in a so-called "sweet spot" where the FRET efficiency is sufficiently high for practicality, but not so high as to suppress time-gated emission by shortening the Tb emission lifetime to within the instrument lag or delay time necessary for measurements. Overall, the initiation of a time-gated FRET cascade with a Tb donor is a very promising strategy for the design, characterization, and application of DNA-based photonic wires and other functional DNA nanostructures.

KEYWORDS: *background rejection, DNA nanotechnology, energy transfer, lanthanide complex, locked nucleic acid, photonic wire*

DNA represents an exciting and promising approach to the bottom-up assembly of nanoscale devices for applications such as light harvesting, optical computing, and biological probes.[1−4] As a building block, DNA is advantageous because of its availability, versatility, and programmability. Long lengths of DNA can be obtained from natural sources, then amplified and modified enzymatically, whereas oligonucleotides can be made by solid-phase chemical synthesis or obtained from commercial vendors with terminal or internal modifications such as functional linkers and fluorescent dyes. Complementary DNA sequences predictably and spontaneously hybridize into relatively rigid double helical structures (persistence length ∼ 50 nm), and the rise of the helix (∼0.34 nm per base pair) affords subnanometer control over length.[1,4,5] Many years of research on DNA assembly have led to creation of a toolbox with concepts such as DNA origami and DNA tiles that enable the sequence-directed construction of complex, multidimensional structures based on Watson−Crick base-pairing and the double-helix motif.[6−10] When decorated with optically active materials such as fluorescent dyes or metal nanoparticles, such DNA nanostructures can serve as scaffolds for optical devices and circuits that range in complexity from one-dimensional wires to two-dimensional "motherboards" or "peg-boards," to more complex three-dimensional photonic architectures.[3,11−16] Many recent reviews have highlighted DNA nanotechnology and its prospective applications.[2,6,9,11,17−24]

An important thrust of DNA nanotechnology research has been the development of DNA-based photonic wires and switches that operate via Förster resonance energy transfer (FRET) cascades.[3,4,24] In these configurations, double-stranded DNA is used as a template to organize a linear array of fluorophores to accept a photon input at one terminus and emit a photon output at the opposite terminus.[1] Excitonic energy is transferred nonradiatively along the length of the wire through a series of n FRET steps, typically between $n + 1$ different fluorophores ordered from shortest to longest wavelengths of absorbance and emission. For example, early work by Kawahara

Received: February 6, 2015
Published: March 27, 2015

DOI: 10.1021/acsphotonics.5b00052
ACS Photonics 2015, 2, 639−652

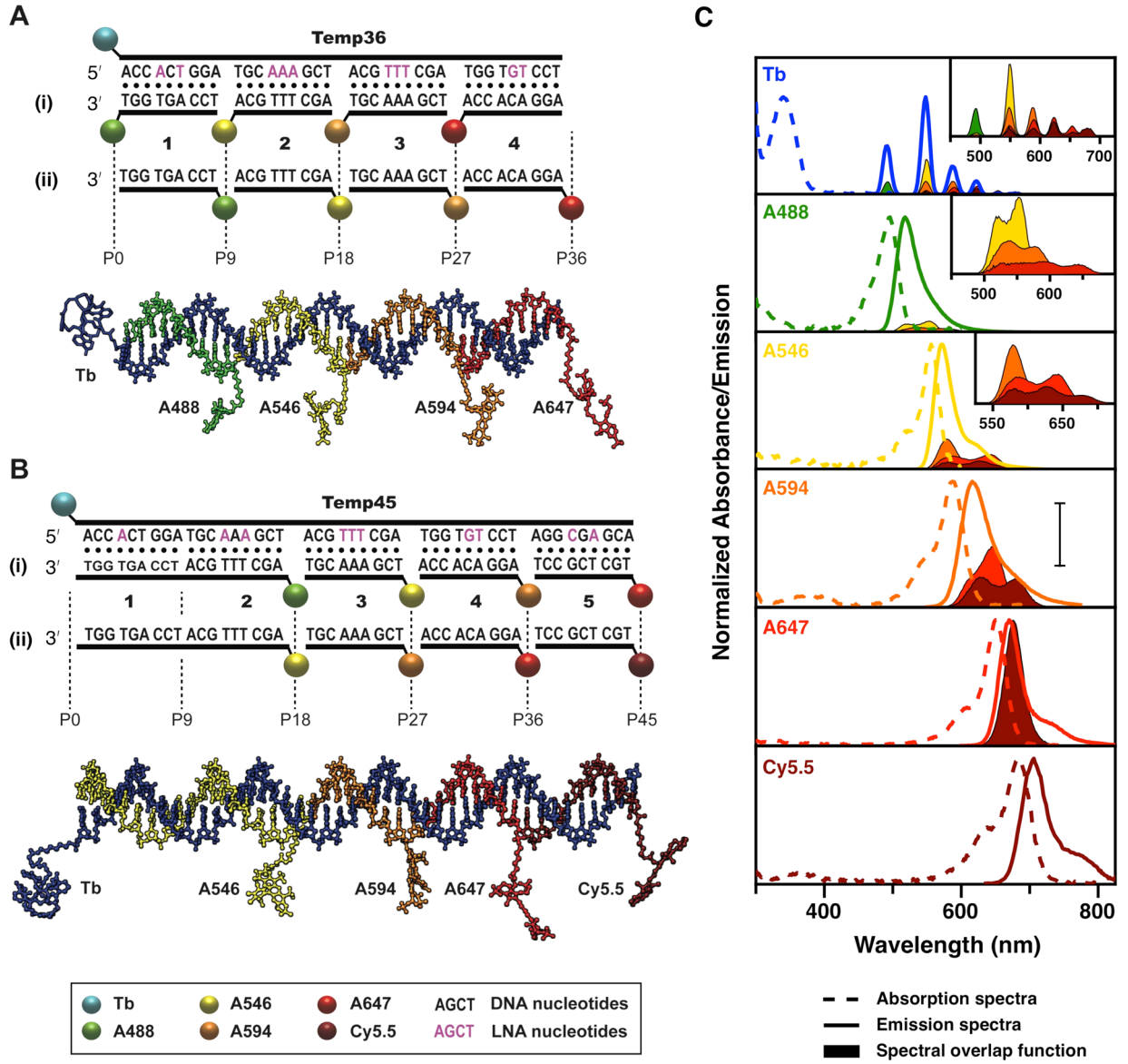

Figure 1. (A) Design of the Temp36 photonic wire, including the nucleotide sequences of the template and complementary segment strands; two arrangements of fluorescent dyes, (i) and (ii), and a model of the photonic wire in (ii). (B) Design of the Temp45 photonic wire, including the nucleotide sequences of the template and complementary segment strands; two arrangements of fluorescent dyes, (i) and (ii), and a model of the photonic wire in (ii). Boldface Arabic numbers are used to denote segment strands and P*n* labels denote dye positions. (C) Normalized absorption (dashed lines) and emission spectra (solid lines) for the Tb and dyes used in this study. Spectral overlap functions for each donor with its potential acceptors are also shown (shaded curves). The spectral overlap functions are scaled relative to one another and color-coded by the acceptor dye. The scale bar (A594 panel) represents a magnitude of 3.5×10^{-11} cm^5 mol^{-1} and applies to all of the main panels. The insets show spectral overlap functions for a given donor on a magnified scale.

et al. demonstrated two-step energy transfer along a DNA wire over ∼8 nm.[25] Subsequent work by Ohya et al.[26] and Heilemann et al.[27,28] demonstrated three- and four-step energy transfer over distances of ∼10 and ∼13 nm, respectively. More recently, Spillman et al. demonstrated a DNA photonic wire with six-step energy transfer over >16 nm.[29] Dynamic DNA structures or "switches" that can interrupt or redirect the flow of energy have also been developed by combining multistep FRET with toe-hold mediated strand invasion.[30] As a potential mechanism for the transmission of information, FRET is advantageous in that it is not diffraction-limited, occurring through-space over nanometer distances, typically on the time scale of nanoseconds or less. However, current DNA-organized FRET-based photonic wires are often nonideal in that they suffer from photobleaching of the constituent dyes, undesirable direct excitation of dyes downstream from the initial dye in the wire, relative orientations of dyes that are neither optimal nor randomized, lower than predicted transfer efficiencies, and sensitivity to partially formed structures in ensemble measurements.[27,29,31] Despite these challenges, the combination of DNA templates, fluorescent dyes, and FRET remains one of the most tractable and promising approaches for designing photonic architectures. One strategy to address the limitations associated with fluorescent dyes is the utilization of alternative materials, which, to date, has largely focused on using semiconductor quantum dots (QDs) as both initial input fluorophores and central scaffolds for integrating multiple photonic wires.[32,33] QDs can potentially confer greater

DOI: 10.1021/acsphotonics.5b00052
ACS Photonics 2015, 2, 639−652

resistance to photobleaching, increase the efficiency and flexibility of photonic input through their spectrally broad and strong absorption, and improve the first energy transfer step through their unique characteristics as FRET donors.[34] Most other photoluminescent materials remain largely unexplored in photonic wire configurations.

Here, we expand the range of materials utilized in DNA-based photonic wires by utilizing a luminescent terbium complex as the initial donor for a multistep FRET cascade along a mixed DNA/locked nucleic acid (LNA) wire. Only single-step FRET with terbium complexes has been previously studied with DNA structures.[35] Luminescent lanthanide complexes are interesting optical materials because of their multiple, narrow emission lines, unpolarized emission, and lifetimes on the order of microseconds to milliseconds.[36,37] Lanthanide complexes have also been reported to have greater photostability than fluorescent dyes.[38,39] Homogeneous time-resolved fluorescence assays have long taken advantage of the extended lifetimes of terbium(III) and europium(III) complexes to reject short-lifetime background fluorescence from measurements and eliminate the need for washing steps to remove excess detection reagents.[40,41] More recent work has demonstrated high levels of multiplexing by pairing different FRET acceptors with the various emission lines of terbium(III) complexes.[42,43] In the context of photonic wires, the unique emission properties of luminescent lanthanide complexes can address some of the limitations of configurations that rely exclusively on conventional organic fluorophores. Using a brightly luminescent terbium(III) cryptate (abbreviated Tb) developed by Raymond's group,[44] we show that a luminescent lanthanide complex can enable time-gated, four-step FRET cascades over DNA photonic wires ~15 nm in length. The goal was not to set a new benchmark for the FRET cascade between conventional organic dyes, but rather to evaluate the utility of an initial Tb donor. The versatility of the multiple emission lines of the Tb is demonstrated by initiating the FRET cascade at two different spectral positions, and the time-gating enables minimization of unwanted background emission from direct excitation of noninitial dyes, from excess dye-labeled DNA strands, or from the sample matrix itself. Another important result is the identification of a "sweet spot" for initiating a time-gated FRET cascade along the photonic wire. This sweet spot represents an optimum balance between either excessive or deficient FRET efficiencies for time-gated measurements with good signal-to-background ratios. The incorporation of LNA residues into our DNA photonic wire has the primary benefit of increasing thermal stability. Overall, we find that the Tb-initiated DNA/LNA photonic wire is an advantageous and highly promising strategy for the design, characterization, and application of DNA nanostructures.

EXPERIMENTAL SECTION

Materials. Dye-labeled and unlabeled DNA oligonucleotides were from Integrated DNA Technologies (Coralville, IA). DNA/LNA template oligonucleotides were from Exiqon (Woburn, MA). Lumi4-Tb-NHS was from Lumiphore (Berkeley, CA). Modified oligonucleotides were HPLC purified by the manufacturer and used as received. Sequences and modifications are shown in Figure 1A,B and listed in the Supporting Information (SI; Table S1). Buffer salts were from Sigma-Aldrich (Oakville, ON). All buffers were filter-sterilized prior to use.

Labeling DNA with Tb. DNA/LNA oligonucleotide template (45.9−65.4 nmol) was dissolved in 250 μL of borate buffer (100 mM, pH 8.5) and 100 μL of DMSO was added. Lumi4-Tb-NHS (0.95−1.14 μmol) was dissolved in 150 μL of DMSO and then added to the DNA/LNA oligonucleotide solution (a final ratio of 1:1 buffer/DMSO). After mixing at room temperature for 14 h, the reaction was diluted with 4 mL of buffer. Oligonucleotide and unreacted Lumi4-Tb-NHS were extracted onto Amberchrom CG300 M resin, eluted with 70% v/v acetonitrile (aq), and dried in a vacuum centrifuge. The residue was then dissolved in 0.2 M triethylamine-acetate buffer (TEAA; pH 7) and the oligonucleotide purified from excess Lumi4-Tb by gel filtration chromatography with Bio Gel P4 media (Bio-Rad, Mississauga, ON). The eluent was concentrated in a vacuum centrifuge, then further purified with a NAP-10 column (GE Health Care, Baie-d'Urfe, QC) using 0.2 M TEAA buffer as the eluent. UV−visible spectrophotometry was used to confirm a Lumi4-Tb/oligonucleotide labeling ratio of ~1:1 and to quantify the amount of product, which was concentrated to dryness and stored at −20 °C until needed.

Hybridization of the Photonic Wire. DNA/LNA and DNA oligonucleotides (i.e., template and complementary segments) were mixed at 1 μM each in tris-borate saline (TBS) hybridization buffer (90 mM tris-borate, 137 mM NaCl, 2.7 mM KCl, pH 7.6), heated to 95 °C for 5 min, then cooled slowly to room temperature. In experiments where dye-labeled oligonucleotides were omitted, unlabeled oligonucleotide segments took their place so that the full length of the template was always double-stranded. Melting experiments are described in the SI.

Emission Measurements. Absorption, excitation, and emission spectra were acquired using a Tecan Infinite M1000 Pro multifunction fluorescence plate reader (Tecan Ltd., Morrisville, NC) using 96-well plates. This instrument utilizes monochromators to select the excitation and emission wavelengths. It can vary the lag time between 0−2000 μs and vary the integration time between 20 and 2000 μs. The excitation wavelength was 355 nm for measurement of prompt and time-gated emission spectra. Lag times were varied depending on the intensity of the prompt background (longer lag times were used for more intense prompt emission) and integration times were varied to maximize signal-to-noise ratios. Typical lag times were between 30 and 50 μs, although some experiments utilized lag times on the order of hundreds of microseconds. In each case, the lag time was found empirically as the minimum time needed to suppress background from prompt dye fluorescence to negligible levels. Integration times were typically hundreds of microseconds (the maximum 2000 μs integration time did not necessarily provide the best signal-to-noise ratios). Specific values for these parameters in a given experiment are indicated in the text or figure captions. The M1000 was also used for measurements of Tb emission decays using a modification of the boxcar method[45] (see SI for details).

Data Analysis. The time-gated emission intensities from each individual dye were determined by spectral decomposition. The base Tb spectrum was scaled using the sample emission intensity between 470−490 nm, which originated exclusively from the Tb, and subtracted to yield the dye-only time-gated emission spectra. The peak emission intensities from each dye were determined from their peak emission wavelengths with crosstalk corrections for the emission tails of preceding dyes in the FRET cascade series.

DOI: 10.1021/acsphotonics.5b00052
ACS Photonics 2015, 2, 639−652

Table 1. Photophysical Properties of the Fluorescent Dyes Used in This Study

dye	$\lambda_{max,\ abs.}$[a] (nm)	ε ($\lambda_{max,\ abs.}$)[b] (M^{-1} cm^{-1})	$\lambda_{max,\ em.}$[c] (nm)	Φ[d]	τ_0[e] (ns)	R_0[f] (nm)				
						A488	A546	A594	A647	Cy5.5
Tb	340	26000	492, 545	0.77	2.6×10^6	4.8	5.5	5.4	5.4	5.1
A488	496	73000	519	0.92	3.1		5.5	5.2	4.8	
A546	556	112000	573	0.79	3.6			6.0	6.1	5.7
A594	590	92000	617	0.66	3.5				6.9	6.6
A647	650	270000	665	0.33	0.74					6.5
Cy5.5	673	209000	707	0.30	0.92					

[a]Wavelength of absorption maximum (for Tb, this value corresponds to the Lumi4 ligand). [b]Molar absorption coefficient at $\lambda_{max,abs}$. [c]Wavelength of emission maximum (only the two most important peaks are listed for Tb). [d]Dye quantum yield (reported by the manufacturer); for Tb, this value corresponds to the Tb^{3+} ion. [e]Emission lifetime. [f]Calculated Förster distance for the donor−acceptor pair indicated. Values for spectral overlap integrals can be found in the SI (Table S2).

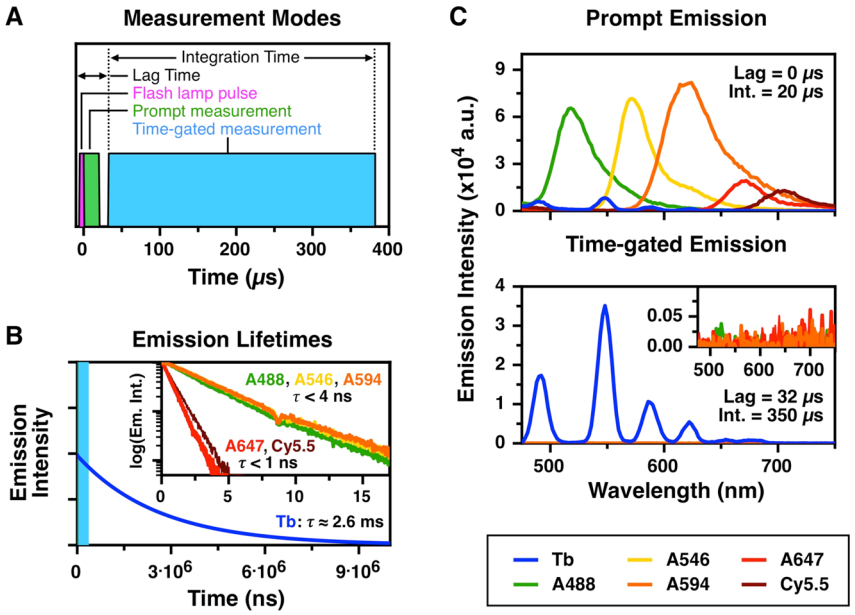

Figure 2. (A) Schematic illustration of prompt and time-gated measurements, showing the pulse of light from the xenon flash lamp and signal acquisition windows, defined by the lag time and integration time, for both modes. (B) Time-resolved emission decay curves for the Tb (main panel; calculated from experimental data) and fluorescent dyes (inset; experimental data). The time-gated acquisition window is shown in the main panel (blue shaded region) for reference. The prompt window is not visible on this scale. (C) Prompt measurements are sensitive to directly excited dye fluorescence (top), whereas time-gated measurements are sensitive to Tb emission and reject directly excited dye fluorescence (bottom). The inset shows a close up of the time-gated dye emission (i.e., baseline noise).

RESULTS

Photonic Wire Configurations and Fluorescent Dyes.

Photonic wires were assembled using long DNA/LNA template strands in combination with two series of shorter, dye-labeled DNA strands that were complementary to segments of the template strand. A 36 nucleotide (nt) template sequence, denoted Temp36, and a 45 nt template sequence, Temp45, were used in the experiments. Temp45 was analogous to Temp36, except for an additional 9 nt appended at the 3′ end of the sequence. Each template was obtained with an aminoalkyl linker at its 5′ terminus for labeling with Tb. Figure 1A,B illustrates the design of the Temp36 and Temp45 sequences and their complementary DNA segment strands. Each complementary DNA segment strand was 9 nt in length, and these strands aligned end-to-end along the template strands. Temp36 thus had four complementary segments and Temp45 had five complementary segments (the first two of which were combined into a single 18 nt complement). The segments are numbered **1**−**5** and were labeled at either their 3′ or 5′ terminus with a fluorescent dye (combined segments are indicated with an arrow; e.g., **1** → **3** is a 27-mer combining segments 1, 2, and 3). The sequence of each segment along the template included a central block of 3 nt, of which 2−3 DNA bases were replaced by LNA bases, and two flanking blocks of 3 nt that included two G/C bases and terminal A/T bases (see Figure 1A,B). The goal of incorporating LNA bases into Temp36 and Temp45 was to stabilize the duplexes formed between the templates and their complementary segment strands, thereby stabilizing the photonic wire structure. Apparent melt temperatures were ≥4 °C higher for Temp45 with LNA bases than without (see SI, Figure S2). Neglecting the flexibility of the linkers between the DNA backbone and a fluorescent dye label, and using canonical double-stranded B-DNA as a structural model, the fluorescent dye labels on two adjacent DNA segments were hypothetically positioned about 3.2−3.3 nm apart.

The fluorescent dyes used in this work were Alexa Fluor 488 (A488), Alexa Fluor 546 (A546), Alexa Fluor 594 (A594), Alexa Fluor 647 (A647), and Cyanine 5.5 (Cy5.5). Pertinent photophysical properties of these dyes are listed in Table 1, and

DOI: 10.1021/acsphotonics.5b00052
ACS Photonics 2015, 2, 639−652

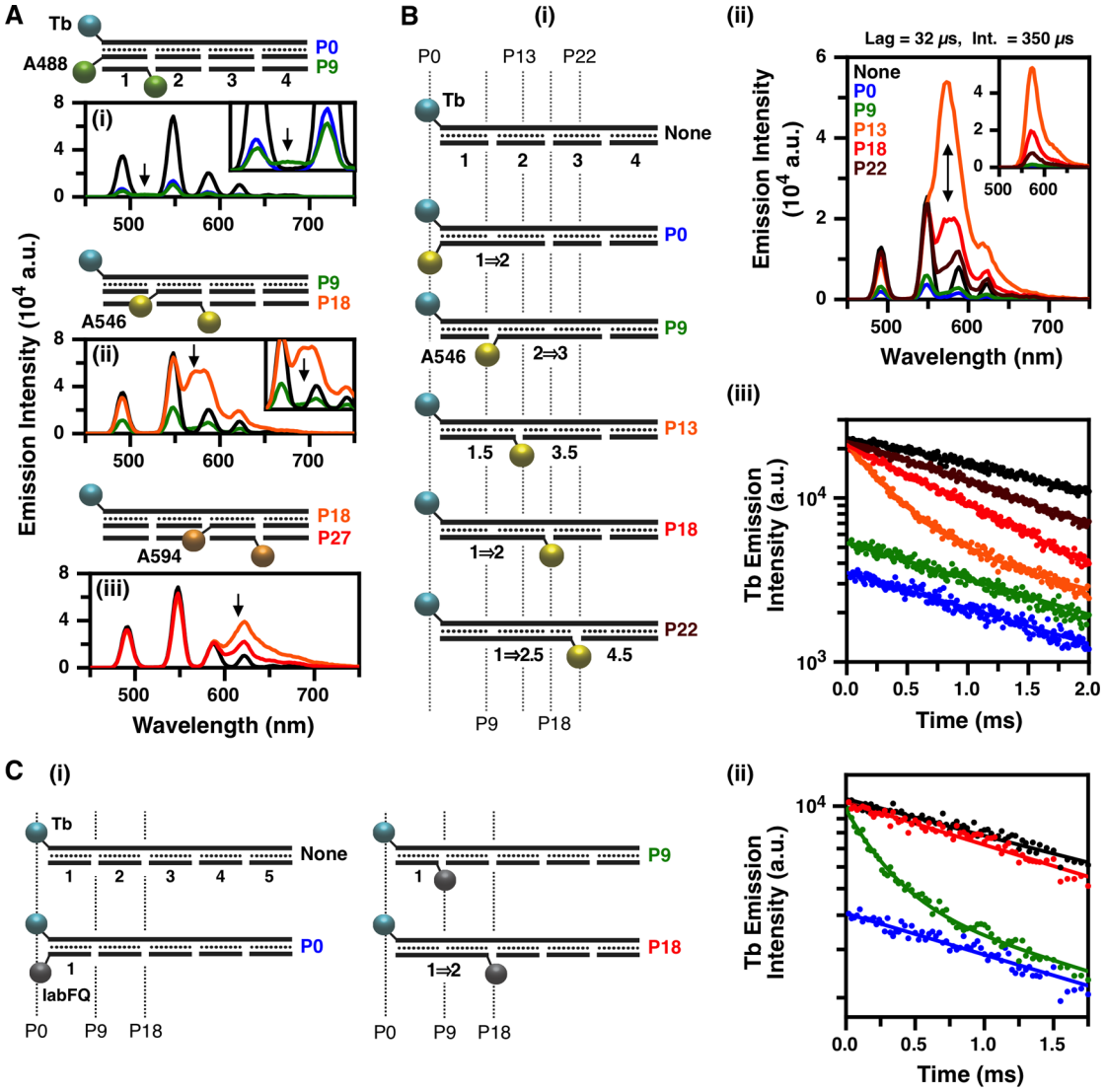

Figure 3. (A) Schemata and time-gated emission spectra (32 μs lag-time; 350 μs integration time) for Temp36-(Tb) hybridized with (i) **1**-(3′A488) and **1**-(5′A488) to place dyes at positions P0 and P9; (ii) **2**-(3′A546) and **2**-(5′A546) to place dyes at positions P9 and P18; and (iii) **3**-(3′A594) and **3**-(5′A594) to place dyes at positions P18 and P27. Arrows indicate the approximate position of the dye emission maximum. The color of the spectra match the color of the P*n* labels. (B) Optimization of dye position for time-gated dye emission. (i) Schemata for configurations with an A546 acceptor at positions P0, P9, P13, P18, and P22 along Temp36-(Tb). The colors of the P*n* labels match the corresponding (ii) time-gated emission spectra (32 μs lag-time; 350 μs integration time) and (iii) Tb PL decay curves for the configurations. The inset in panel (ii) shows the time-gated emission spectra with the Tb contribution subtracted. (C) Experiment analogous to that in (B), with a dark quencher rather than a fluorescent dye. (i) Schemata for configurations with an IabFQ acceptor at positions P0, P9, and P18 along Temp45-(Tb). The colors of the P*n* labels match the corresponding (ii) Tb PL decay curves.

absorption and emission spectra for each dye are shown in Figure 1C with the corresponding spectral overlap functions for each FRET pair in this study. Förster distances for the FRET pairs are also listed in Table 1, calculated with the assumption that the dipole orientation factor for energy transfer (κ^2) is equal to 2/3. For this assumption to hold, fast isotropic motions of the dyes are required.[46] In the photonic wire configurations, the fluorescent dyes can be located at the positions shown in Figure 1A,B. These positions are referred to as P*n*, where *n* represents the number of nucleotides between the attachment position of the Tb and the attachment position of the dye (e.g., P9 refers to a separation of 9 nt between the Tb and the dye). It should be noted that, with the exception of the termini of a template sequence, dyes can be located in a given position by labeling either the 5′ terminus of one complementary segment or the 3′ position of the adjacent complementary segment. In the full photonic wire configurations, the approximately 3.2−3.3 nm separation between nearest-neighbor dyes is predicted to yield FRET efficiencies >95%. When necessary for experiments, different dye−dye or Tb−dye combinations were isolated by using unlabeled template or unlabeled complementary segment strands, thereby maintaining consistent double-stranded structure along the entire length of the DNA photonic wire. In the following sections, photonic wire configurations and their components will often be referenced using the template abbreviations, numbered segments, dye abbreviations, and P*n* dye positions.

Another important feature of the current photonic wire design is the mismatch between the ∼2.6 ms emission lifetime of the Tb[47] and the <4 ns lifetimes of the fluorescent dyes. It is

DOI: 10.1021/acsphotonics.5b00052
ACS Photonics 2015, 2, 639−652

the extraordinarily long lifetime of the Tb that permits time-gated measurements, the concept of which is illustrated in Figure 2A. A pulse of light from a xenon flash lamp excites the sample and emission is measured after a defined delay or lag time, for a duration defined by the integration time, where both quantities are on the order of tens to hundreds of microseconds. Figure 2B shows the time-resolved emission decays for the Tb and fluorescent dyes, with the precise lifetimes listed in Table 1. Figure 2C illustrates the effect of time-gating. Prompt, directly excited emission from the dyes in the photonic wire (defined here as being measured with a 0 μs lag-time and a 20 μs integration time) is much more intense than the Tb emission, even when excited at 355 nm, which is not an optimal wavelength for maximum excitation of the dyes (see Figure 1C). The Tb emission is weak because its emission is spread over milliseconds. With time-gating (32 μs lag-time) and a longer integration time (350 μs integration time), the Tb emission is measured with much improved signal-to-noise, and the directly excited dye emission decreases to background levels. The prompt measurement captures an estimated 0.7% of the total native Tb emission (i.e., unquenched by FRET), whereas the above time-gated measurement captures ∼12% of the total emission. It should be noted that the 32 μs lag time is needed to allow not only the prompt emission to reach background levels, but also to allow the flash lamp afterglow and residual detector signal from the intense prompt emission to subside.[48] The prompt measurement captures ∼100% of the native dye emission (i.e., not FRET-sensitized) and the time-gated measurement captures ∼0%.

Optimal Position of the Initial Dye. To enhance time-gated sensitization of the dye-to-dye FRET cascade along the photonic wire, our first inclination was to maximize the FRET efficiency between the initial Tb donor and the first fluorescent dye in the series by minimizing their separation distance. To this end, Temp36-(Tb) (see Figure 1A) was hybridized with segment **1**-(3′A488) so as to place the dye at position P0, or segment **1**-(5′A488) so as to place the dye at position P9, where all other segment strands were unlabeled. As shown in Figure 3A(i), both of these configurations quenched the time-gated Tb emission intensity by >80%. No detectable time-gated A488 emission was observed from **1**-(3′A488), and only a miniscule amount was observed from **1**-(5′A488), which placed the dye at position P9. Figure 3A(ii) shows that segment **2**-(3′A546), which also placed the dye at position P9, quenched the time-gated Tb emission by ∼70% but still yielded only a small amount of time-gated A546 emission. In contrast, **2**-(5′A546) and **3**-(3′A594), which placed dyes at position P18, yielded intense time-gated dye emission, as shown in Figure 3A(ii,iii). At the subsequent P27 position along Temp36-(Tb), segment **3**-(5′A594) also yielded significant time-gated dye emission, as shown in Figure 3A(iii). Apparent quenching of the time-gated Tb emission was notably less (≤10%) in the configurations with significant time-gated dye emission.

Given the foregoing data, and the absence of any anomalous quenching of the prompt A488 and A546 emission when located at positions P0 and P9, we hypothesized that FRET was too efficient for time-gated measurements when acceptor dyes were located at these positions. As the FRET efficiency, E, increases, the Tb donor emission lifetime is expected to decrease according to eq 1, where τ_{DA} and τ_D are the Tb lifetimes in the presence and absence of dye acceptor.[46]

$$E = 1 - (\tau_{DA}/\tau_D) \quad (1)$$

The Tb is reported to have an unquenched lifetime of ∼2.6 ms[47] and, according to eq 1, a FRET efficiency greater than 95% would reduce the Tb lifetime to less than 100 μs. Under these conditions, a majority of the Tb emission would then occur within the measurement lag time rather than the integration time. Since the emission lifetimes of the dyes were less than 4 ns, the Tb lifetime determines the time scale of FRET-sensitized, time-gated dye emission. Acceptor dye emission within the lag-time rather than the integration time is consistent with the negligible time-gated emission from **1**-(3′A488) (dye at P0) and minimal time-gated emission from **1**-(5′A488) and **2**-(3′A546) (dye at P9), as observed in Figure 3A. Consideration of the integration time and lag time with respect to eq 1 also provides an explanation for the minimal quenching of the Tb emission in configurations with significant FRET-sensitized dye emission (vide infra).

To test the above hypothesis, a set of configurations were prepared where A546 was moved along Temp36-(Tb) from position P0 stepwise through to position P22, using the complementary segment strands **1** → **2**-(3′A546), **2** → **3**-(3′A546), **1.5**-(5′A546), **1** → **2**-(5′A546), and **1** → **2.5**-(5′A546), as shown in Figure 3B(i). The half segment numbers refer to sequences that were extended by less than a 9 nt unit (see Table S1 for sequences). Combining the segments as single dye-labeled complementary strands of at least 14 nt simplified the experiment and increased duplex stability. Unlabeled segments were used to complete the double-stranded structure along Temp36-(Tb). The time-gated A546 emission (32 μs lag, 350 μs integration time), shown in Figure 3B(ii), scaled as P13 > P18 > P22 ≫ P9 > P0. In contrast, quenching of the Tb emission scaled as P0 > P9 ≫ all other positions, consistent with the hypothesis that very efficient FRET can shift sensitized A546 emission to shorter times that are outside of the measurement window.

To directly confirm significant shortening of the Tb lifetime with FRET, the PL decay of Tb was measured for each configuration in Figure 3B(i). As shown in Figure 3B(iii), the Tb had a lifetime of ∼2.7 ms in the absence of A546, consistent with previous measurements.[47] With **1** → **2.5**-(5′A546) at P22 and **1** → **2**-(5′A546) at P18, the Tb lifetime decreased to ∼1.7 and ∼1.2 ms, respectively, and retained monoexponential character. Interestingly, for **1.5**-(5′A546) at P13, the Tb PL decay had biexponential character with a ∼380 μs component (73%) and a residual 2.7 ms component (27%). As the A546 was moved closer to the Tb with **2** → **3**-(3′A546) at P9 and **1** → **2**-(3′A546) at P0, the strongly quenched Tb emission returned to an apparent monoexponential decay with lifetimes >2 ms. The strong quenching of the Tb is hidden within the first few microseconds of the decay curve and the time-gate. This result is consistent with previous observations of quenching of Tb PL via FRET with a residual native Tb lifetime component.[42,43,47,49,50]

For FRET associated with **1** → **2**-(5′A546) at P18 and **1** → **2.5**-(5′A546) at P22, the faster decay of the Tb in Figure 3B(ii) was such that a greater percentage of the total Tb PL was within the integration time. For the unquenched Tb, the lag time and integration time combination measured ∼12% of the total Tb PL, whereas ∼18% and ∼24% of Tb PL were measured for A546 at P22 and P18, respectively. Some of the FRET-induced quenching of the Tb was thus offset, and the measured Tb PL intensities for A546 at P18 and P22 were expected to be within 10% of the Tb alone, as observed experimentally. For **1.5**-(5′A546), ∼30% quenching of Tb PL

DOI: 10.1021/acsphotonics.5b00052
ACS Photonics 2015, 2, 639−652

was expected to be observed in time-gated measurements, albeit that this quenching was convoluted with residual unquenched Tb PL and some overlap with A546 emission in Figure 3B(ii).

To ensure the generality of the above results, a similar experiment was done with Iowa Black FQ (IabFQ), a dark quencher, instead of A546, where the Förster distance for the Tb-IabFQ FRET pair was 5.1 nm (cf. 5.5 nm for Tb-A546). As shown in Figure 3C, a similar trend in the Tb lifetime was observed when Temp45-(Tb) was hybridized with **1**-(3′IabFQ), **1**-(5′IabFQ), and **1** → **2**-(5′IabFQ), placing the IabFQ quencher at P0, P9, and P18, respectively. The **1**-(3′IabFQ) at P0 had strongly quenched Tb emission with a lifetime (2.9 ms) indistinguishable from the Tb alone (2.9 ms), the **1**-(5′IabFQ) at P9 had a biexponential Tb decay with a fast FRET-quenched component (280 μs, 53%) and a residual native component (2.9 ms, 47%), and the **1** → **2**-(5′IabFQ) at P18 had a quenched apparent monoexponential Tb decay (2.8 ms). The onset of the biexponential decay at a shorter donor–acceptor distance than with A546 (P9 vs P13) is consistent with the shorter Förster distance associated with IabFQ.

Lastly, the Tb and A546 emission was measured as a function of lag time (with a fixed 50 μs integration time) for Temp36-(Tb) hybridized with **1**-(5′A546), **1** → **2**-(5′A546), **1** → **3**-(5′A546), and **1** → **4**-(5′A546), corresponding to P9, P18, P27, and P36. The trends in the data (see SI, Figure S3) were analogous to the trends in the Tb lifetime data (Figure 3B), with the important observation that the A546 emission tracked with the Tb emission, as expected given the million-fold difference in lifetime. Although there was virtually no A546 emission with **1**-(5′A546) at P9 after a 50 μs lag time, the prompt A546 emission from **1**-(5′A546) was more intense than for the other segments at lag times <30 μs. This result was consistent with efficient FRET-sensitized emission from **1**-(5′A546) being convoluted with directly excited prompt **1**-(5′A546) emission over the prompt time scale (0 μs lag; 20 μs integration time) of our instrument.

Cumulatively, the above data confirm that highly efficient FRET between Tb and dyes at positions P0 and P9 reduces the Tb emission lifetime to a time scale comparable to the instrument response to prompt emission, thereby preventing resolution of time-gated Tb-sensitized emission from the acceptor dyes. Positioning the first acceptor dye further from the Tb, at position P13 or P18, overcomes this problem. These results will be discussed below in the context of a "sweet spot" for energy transfer.

Assembly of the Time-Gated Photonic Wires. As shown in Figure 1B, two different photonic wires were assembled with the initial acceptor dye at position P18. Although position P13 yielded greater FRET, position P18 was utilized in photonic wire experiments to permit use of interchangeable 9 nt oligonucleotide segments. The first of the photonic wires, shown in Figure 1B(i), features a FRET cascade, Tb → A488 → A546 → A594 → A647, where the arrow indicates the direction of energy transfer. The second of these wires, shown in Figure 1B(ii), features a FRET cascade from Tb → A546 → A594 → A647 → Cy5.5. These configurations differed only in the selection and positioning of the dye labels, as the same template and segment strand sequences were utilized. For brevity, the configuration in Figure 1B(i) is referred to as the Tb/A488-initiated wire, and the configuration in Figure 1B(ii) is referred to as the Tb/A546-initiated wire.

The first energy transfer step in the photonic wire is from the Tb to the first fluorescent dye down the length of the template. For the two configurations in Figure 1B, the first dye is either (i) A488 or (ii) A546. To estimate the FRET efficiency from the Tb to the first dye, the change in the decay rate of the Tb was measured. Previous studies have found that quenching of the Tb PL intensity is not necessarily a reliable measure of FRET efficiency because the lag time and integration time do not capture the full decay of the Tb emission (see SI for details), whereas changes in lifetime are reliable.[34,37,42,43,47,49,50] Figure 4 shows changes in the Tb emission decay upon the addition of an initial A488 or A546 acceptor, measured using the aforementioned boxcar technique. In this experiment, the Tb emission lifetime was calculated to be ∼2.5 ms for the Temp45-(Tb) conjugate, consistent with Figure 3B and the 2.6 ms lifetime previously reported.[47] The Tb lifetime decreased to ∼1.8 and ∼1.2 ms with A488 and A546 acceptors, respectively, corresponding to FRET efficiencies of ∼28% and ∼52% (calculated via eq 1). These FRET efficiencies translate into average donor–acceptor separations of ∼5.6 and ∼5.4 nm, which are in reasonable agreement with the ∼6.0 nm separation distance expected from simple geometric considerations for B-DNA (without considering the flexibility of the linkers between the dyes and the oligonucleotides). The larger FRET efficiency for the Tb-A546 pair arises from the larger spectral overlap integral and longer Förster distance (see Table 1).

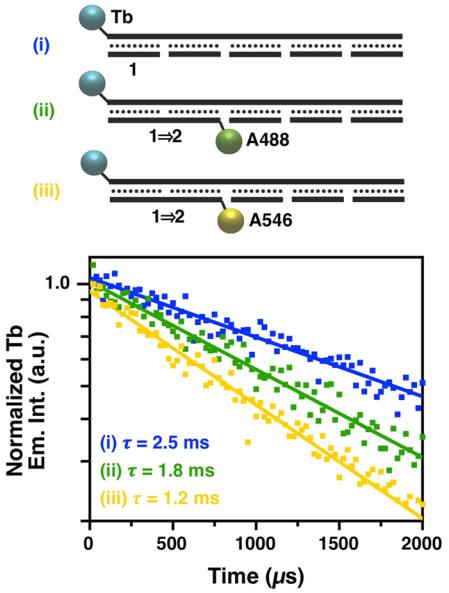

Figure 4. Schemata and decay curves for configurations with (i) only Tb, or a single energy transfer step from the Tb to (ii) A488 or (iii) A546 at P18.

Figure 5 shows changes in the prompt (0 μs lag-time, 20 μs integration time) and time-gated emission spectra (32 μs lag-time, 350 μs integration time) with stepwise assembly of both the Tb/A488-initiated and Tb/A546-initiated photonic wire configurations. The prompt spectra show quenching of each nth dye with the addition of the $(n + 1)$th dye along Temp45, and concomitant sensitized emission from the $(n + 1)$th dye. The latter is mixed with directly excited $(n + 1)$th dye emission, estimates of which were obtained from samples with only one dye-labeled segment strand and are also shown in Figure 5. The time-gated spectra show a similar progression of FRET-induced

DOI: 10.1021/acsphotonics.5b00052
ACS Photonics 2015, 2, 639–652

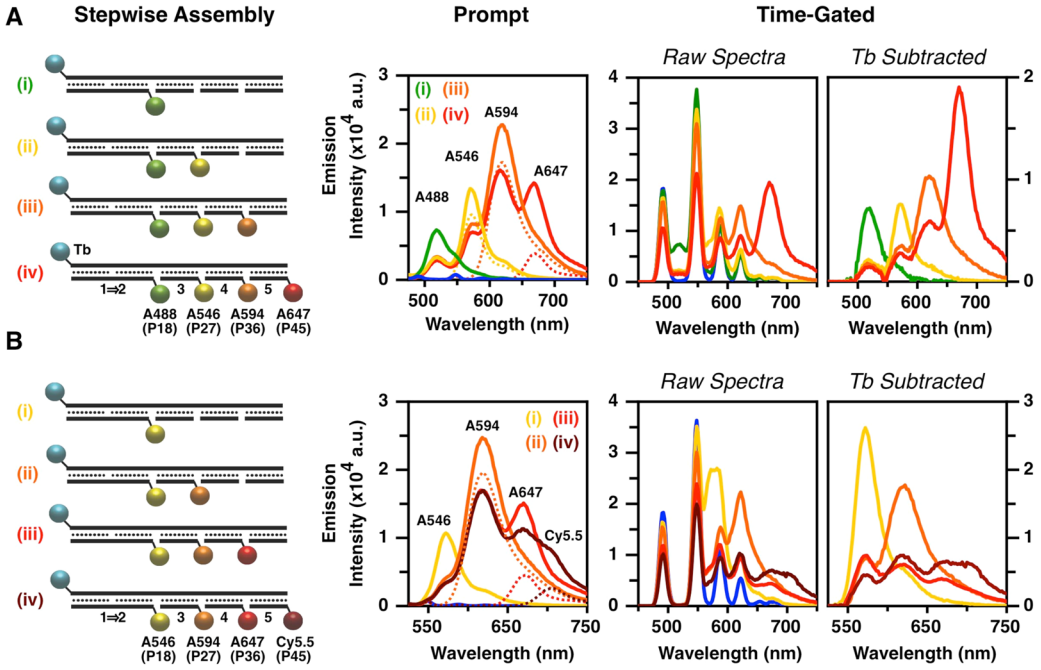

Figure 5. (A) Evolution of the FRET cascade in the Tb/A488-initiated photonic wire depicted in Figure 1B(i) from left to right: stepwise assembly of the full photonic wire; representative prompt emission spectra (estimated direct excitation components are shown as dashed lines and arise from the UV absorption of the dyes); representative raw time-gated emission spectra; and corresponding Tb-subtracted time-gated emission spectra. The colors of the spectra correspond to the colors of the lowercase Roman numeral labels. (B) Analogous data for the FRET cascade in the Tb/A546-initiated photonic wire depicted in Figure 1B(ii). In both cases, the lag time and integration time were 32 and 350 μs, respectively, for time-gated measurements. A 20 μs integration time was used for prompt measurements.

quenching and sensitization of the nth and $(n + 1)$th dyes, which is more readily apparent when the Tb emission has been subtracted from the overall spectrum. In the case of time-gating, there is no directly excited dye emission (vide infra), and thus, the time-gated emission spectra have a different shape than the corresponding prompt spectra (i.e., different magnitudes of emission from each dye). The time-gated spectra are reflective of end-to-end energy transfer along the photonic wire, whereas the prompt spectra represent a composite of energy transfer resulting from energy input at multiple points along the wire.

To further characterize the photonic wires, time-gated emission spectra were measured, in triplicate, for each permutation of the two configurations. These permutations included four variations with one dye, six variations with two dyes, four variations with three dyes, and the full configuration with four dyes in series. Representative spectra for each configuration are shown in the SI (Figures S4 and S5). FRET efficiencies between the various dyes were calculated, using eq 2,[46] from the quenching of their time-gated intensities, I_X, when an acceptor (DA) was added to an otherwise analogous configuration (D). The various donor−acceptor efficiencies are plotted in Figure 6A. Quenching of the time-gated fluorescence intensity of dye donors provides an accurate measure of the FRET efficiency between dyes because their decay occurs within a time period >10^4-fold shorter than the integration time. Within the precision of the experiments, the apparent FRET efficiency between the nth and $(n + 1)$th dye were insensitive to the presence or absence of the $(n + 2)$th dye. For example, in the case of Tb/A488-initiated wire, quenching of A488 by A546 with energy transfer between positions P18 and P27 was not significantly affected by the presence of A594 at position P36. The nearest-neighbor FRET efficiencies ranged from about 30−80%, most of which were markedly less than the ∼95% quenching efficiency predicted from Förster distances and positioning along the dsDNA helix. The end-to-end FRET efficiency from the dye at P18 to the dye at P45 (∼9 nm) was 22 ± 6% for the Tb/A488-initiated wire and 16 ± 5% for the Tb/A546-initiated wire. These values decreased to 6 ± 2% and 8 ± 3%, respectively, when considering energy transfer from the Tb at P0 to the dye at P45 (∼15 nm). Rates of FRET, k_{FRET}, were calculated from eq 3[46] and are summarized in Figure 6B. These rates varied from 10^8 to 10^9 s^{-1} for nearest-neighbor FRET pairs, and 10^7 to 10^8 s^{-1} for next-nearest-neighbor FRET pairs. For comparison, the calculated rates for the initial Tb → A488 and Tb → A456 energy transfer steps were about 150 and 400 s^{-1}, respectively, because of the long lifetime of the Tb excited state.

$$E = 1 - (I_{DA}/I_D) \tag{2}$$

$$k_{FRET} = \frac{E}{\tau_0(1 - E)} \tag{3}$$

Rejection of Background Signals by Time-Gating. Unwanted background fluorescence during the measurement of photonic wire emission can arise from multiple sources. One such example is the direct excitation of dyes along the photonic wire that are not the initial donor, resulting in a heterogeneous distribution of FRET cascades initiated at different points along the wire. In addition, directly excited fluorescence from excess dye molecules (i.e., not integrated into a photonic wire structure) may distort or swamp out measured emission spectra. Background fluorescence may also be associated with the medium for the photonic wire. As illustrated in Figure 7, time-gated emission measurements can help ameliorate each of these three potential issues. Figure 7A shows prompt and time-gated excitation spectra for the terminal A647 acceptor as the

DOI: 10.1021/acsphotonics.5b00052
ACS Photonics 2015, 2, 639−652

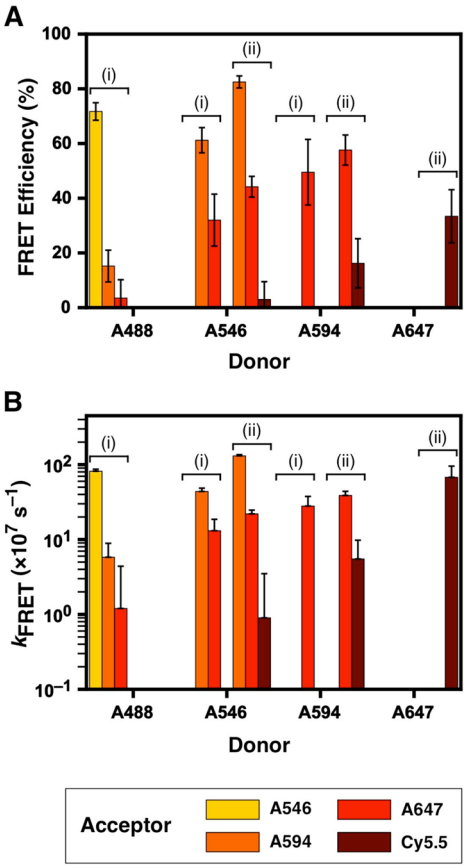

Figure 6. (A) Efficiencies for time-gated FRET between dyes in the photonic wire configurations. The labels (i) and (ii) indicate the configuration in Figure 1B. For reference, the Tb → A488 and Tb → A546 FRET efficiencies are 28% and 52%, respectively. (B) Rates of FRET between the dyes in the photonic wire configurations. For reference, the Tb → A488 and Tb → A546 FRET rates are 150 and 400 s^{-1}, respectively.

Tb/A488-initiated photonic wire is assembled in reverse; that is, starting from the terminal A647 acceptor with the progressive addition of each dye before it in the FRET cascade, with the initial Tb donor present in all cases. The prompt spectra show a progressive convolution of the excitation spectra of each dye, demonstrating the potential initiation of the FRET cascade at multiple points along the photonic wire. In contrast, the time-gated excitation spectra show only the excitation profile of the Tb, which generally increases in magnitude as the wire is assembled in full, consistent with initiation of the time-gated FRET cascade only at the Tb. Analogous data for the Tb/A546-initiated wire is shown in the SI (Figure S6). Figure 7B shows changes in the prompt and time-gated A488 or A594 emission as **1** → **2**-(5′A488) or **3**-(5′A594) was mixed with the other components of the Tb/A488-initiated photonic wire (Figure 1B) at ratios of 1:1, 2:1, 4:1, and 8:1. Ideally, a 1:1 ratio corresponds to the stoichiometric assembly of the photonic wire. Over this range of stoichiometry, the prompt A488 and A594 emission increased by close to an order of magnitude; however, the time-gated A488 and A594 emission increased by less than 2-fold. Finally, Figure 7C shows the prompt and time-gated emission spectra for the stepwise assembly of the A488-initiated photonic wire in 50% v/v serum. The prompt spectra show the emission of the dyes superimposed on a background of serum autofluorescence that is comparable in magnitude. In contrast, the time-gated spectra have a near-zero background with no detectable autofluorescence from the serum.

DISCUSSION

Time-Gated FRET "Sweet Spot". One of the most interesting aspects of this study is finding a "sweet spot" along the photonic wire for optimal time-gated energy transfer between the Tb and the initial dye in the FRET cascade. Specifically, this sweet spot appeared to be between dye positions P9 and P18 in Figure 1. Although other dye positions are in closer proximity to the Tb, the increased FRET efficiency yields a drastic reduction in the Tb lifetime, resulting in sensitized dye emission within the lag time of the instrument used for time-gated measurements. Use of a shorter lag time is precluded by the residual signal from the intense prompt dye emission. Such residual signal is not unique to our fluorescence plate reader, but was also observed with a streak camera system and has been reported in the literature with other instruments.[48] Conversely, positions further away from the Tb than position P18 yield much smaller amounts of time-gated dye emission because of the distance dependence of FRET. The optimum balance between these two opposing effects can be predicted from Förster theory using eqs 4 and 5, where D^* and A^* are the probabilities that the Tb donor and dye acceptor are in an excited state, τ is an excited state lifetime, and $\gamma \equiv (R_0/r)^6$ is the Förster coupling. The time-gated dye emission and its dependences on lag time and integration time can be predicted by solving these equations with suitable initial conditions (see SI for details).

$$\frac{dD^*}{dt} = -\frac{D^*}{\tau_D}(1+\gamma) \tag{4}$$

$$\frac{dA^*}{dt} = -\frac{A^*}{\tau_A} + \frac{\gamma D^*}{\tau_D} \tag{5}$$

Figure 8A shows the predicted dye emission as a function of lag time and relative donor−acceptor separation, r/R_0. The experimental data in Figure 3B is compared to the prediction in Figure 8B. The prediction shows good agreement with the data for dye positions P13 through P36 ($r/R_0 > 0.75$), but overestimates the emission observed at shorter distances, specifically position P9 ($r/R_0 \approx 0.6$), which has almost no time-gated emission. The discrepancy in the case of P9 may be because the actual Tb-dye separation is smaller than the nominal ~3.2 nm, perhaps as a result of the linker lengths (~1 nm) and molecular dimensions (~1 nm) allowing the Tb and dye to approach one another more closely or even associate. At such close proximity, there are two prospective FRET pathways that could shift the sensitized dye emission within the instrument lag time. The first of these pathways is the lanthanide-to-dye energy transfer discussed to this point, which would approach 99% efficiency and reduce the Tb lifetime to <30 μs at separations <2.6 nm (a mere 0.6 nm less than the nominal distance). The second of these FRET pathways is direct cryptand-to-dye energy transfer, which would bypass the lanthanide ion and occur within nanoseconds rather than over microseconds or milliseconds (see SI for discussion). Contributions from this pathway would increase as the Tb-dye separation distance decreases. The balance of the competition between lanthanide-to-dye energy transfer and hypothetical cryptand-to-dye energy transfer is a topic for future research.

DOI: 10.1021/acsphotonics.5b00052
ACS Photonics 2015, 2, 639−652

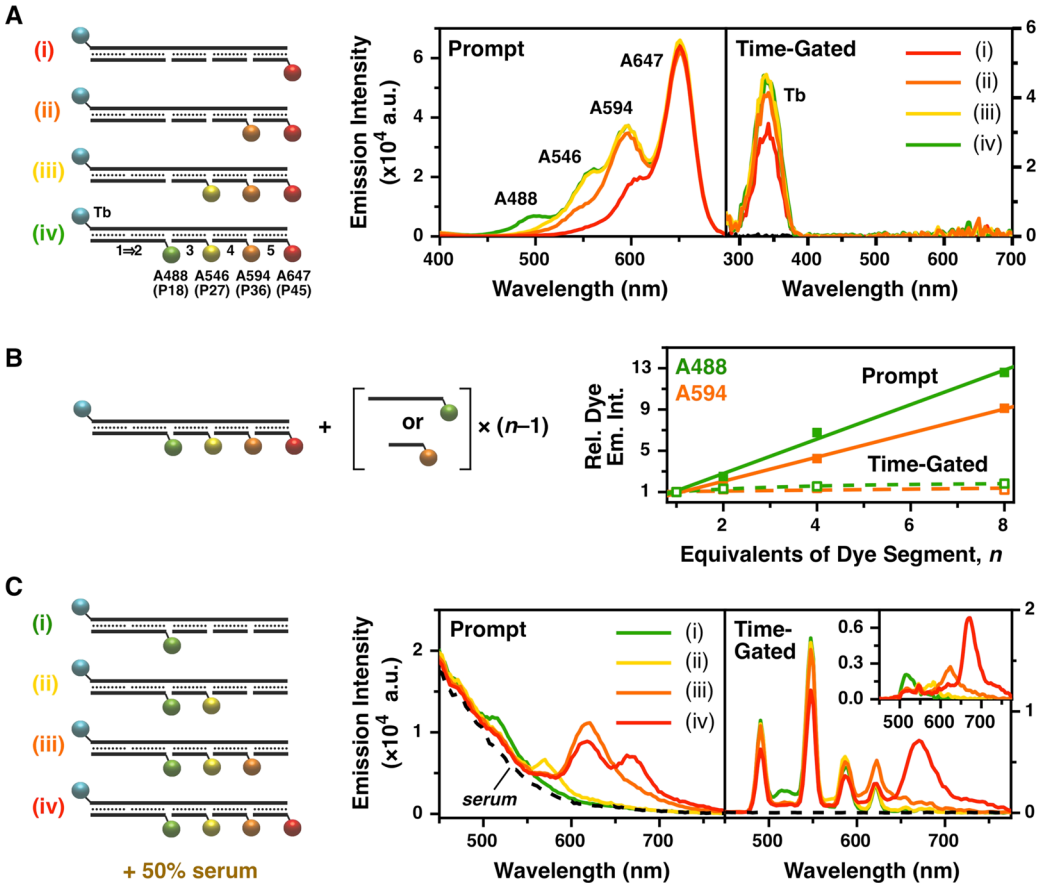

Figure 7. (A) Schematic, prompt, and time-gated excitation spectra for A647 during the reverse stepwise assembly of the Tb/A488-initiated photonic wire depicted in Figure 1B(i). The time-gated settings were 40 μs lag time and 350 μs integration time. (B) Schematic and changes in the prompt and time-gated emission intensities of A488 and A594 with the addition of excess **1** → **2**-(5′A488) or **3**-(5′A594) strands to the full Tb/A488-initiated photonic wire configuration. The lag times and integration times were 40 and 350 μs and 600 and 500 μs, respectively, for the A488 and A594 measurements. (C) Schematic, prompt, and time-gated emission spectra for stepwise assembly of the Tb/A488-initiated photonic wire in the presence of 50% bovine serum. The excitation wavelength was 355 nm. The time-gated settings were 32 μs lag time and 350 μs integration time. The inset shows the time-gated spectra without the Tb emission.

More generally, "sweet spots" should be expected in many other time-gated FRET configurations, especially if the lanthanide complexes have shorter lifetimes than the Tb(III) cryptate used here. In addition to the idea of a time-gated photonic wire, this concept has important implications for the design of time-resolved assays, biosensors, and diagnostics. The closest possible proximity between donor and acceptor may not maximize time-gated signal, which is counter to typical strategies for maximizing prompt FRET. The "sweet spot" effect, which we have shown to be largely predictable from Förster theory, may have received little attention to date because large lanthanide donor-dye acceptor distances have been unavoidably imposed by proteins in time-resolved assays,[41,43] and by nanoparticle radii in other recent studies.[42,51]

Inclusion of LNA Bases. The photonic wire used to evaluate time-gating with an initial Tb donor was simple in its design. Dye-labeled complementary segments were 9 nt in length to provide close proximity between adjacent dyes in the FRET cascade and still permit a single terminal label per oligonucleotide. LNA bases were incorporated into the template oligonucleotides as an a priori measure to improve the thermal stability of the short double-stranded hybrid segments, and to help ensure hybridization of complementary segments exclusively at the intended positions along the template. LNA bases restrain the conformational freedom of DNA strands through a methylene bridge between the 2′ oxygen and 4′ carbon of the ribose ring, resulting in better selectivity against mismatched sequences and tighter binding between complementary sequences (T_m increases by 1−8 °C per LNA nucleotide).[52] To date, LNA and other xeno nucleic acids such as peptide nucleic acid (PNA) have received little attention in the context of DNA nanotechnology, but their structural and functional differences versus DNA (e.g., thermal stability, resistance to enzymatic degradation, degree of tolerance for mismatches)[53,54] could provide important new opportunities. In our experiments, inclusion of LNA bases in the photonic wire template strand afforded greater thermal stability to the hybrid segments than a DNA-only template (Figure S2). Although statistically significant differences in FRET efficiency or acceptor/donor emission ratios were not observed between LNA/DNA and DNA-only templates at room temperature, significant differences were observed at elevated temperature (e.g., physiological temperature; see SI, Figure S2). Inclusion of LNA bases in photonic wires is also expected to increase their resistance to nuclease degradation.[55,56] Given our focus on time-gating, more detailed experiments investigating the effect of LNA on formation of the photonic wire were beyond our scope. Nonetheless, the utility of LNA in photonic wires and other DNA nanostructures warrants further investigation in future studies. LNA bases

DOI: 10.1021/acsphotonics.5b00052
ACS Photonics 2015, 2, 639−652

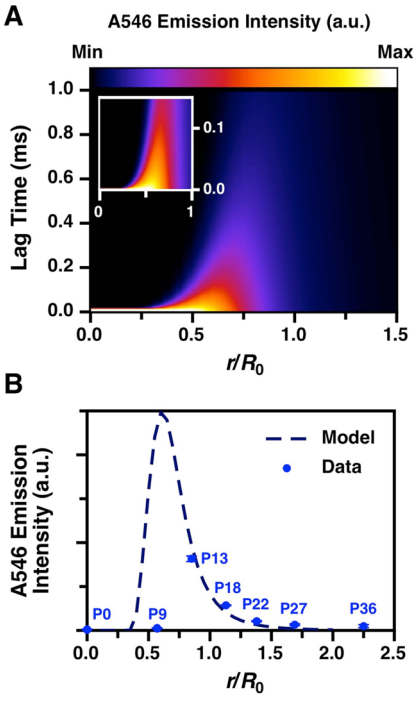

Figure 8. (A) Plot of the predicted time-gated A546 emission intensity as a function of lag time and Tb-A546 separation, r/R_0, for an integration time of 350 μs. The model clearly predicts a "sweet spot." The inset shows a close up of short lag times and small relative donor–acceptor separations. (B) Plot of the experimentally measured, time-gated A546 emission intensities (points; error bars from three replicate data sets are too small to see). The dashed line shows the prediction from (A) for a lag time of 32 μs (to match the experiment).

could, for example, allow the formation of photonic wires at lower ionic strength, higher temperatures, or with shorter oligonucleotide segments.

FRET along the Photonic Wires. Our results clearly demonstrate that Tb can initiate a FRET cascade between a series of fluorescent dyes. It is perhaps surprising, given the Tb-dye separation that corresponds to the "sweet spot," that the efficiency of the initial Tb-to-dye FRET step was not limiting. For the A546-initiated wire, the ~52% Tb → A546 energy transfer efficiency was comparable to the efficiencies for nearest-neighbor A594 → A647 FRET, and better than the efficiency for A647 → Cy5.5. This efficiency was also better than the next-nearest-neighbor FRET efficiencies between dyes, despite occurring over the same putative donor–acceptor separation. Similarly, for the A488-initiated wire, the ~28% Tb → A488 energy transfer is comparable to that observed for A647 → Cy5.5, even though the latter occurs over half the distance. These results suggest that the Tb is relatively well behaved as a FRET donor, whereas the fluorescent dyes underperform in the two FRET cascades. Dye performance less than predicted has been reported in prior studies of photonic wires without time-gating, only some of which can be attributed to incompletely formed structures across an ensemble.[27−29,32,33] Given that Figure S2 suggests no large differences in room temperature hybridization efficiency between the **1** + **2** segment and the **3**, **4**, or **5** segments, we speculate that the unpolarized emission dipole of the Tb yields more favorable orientation factors for Tb-dye FRET pairs than is possible for dye–dye FRET pairs, which may be constrained in their relative orientations. The general and often unjustified assumption of an orientation factor of $\kappa^2 = 2/3$ for dynamically random dye orientations may be an overestimate if the fluorescent dyes physically associate with the DNA photonic wire,[57] or have sterically restricted motion. In contrast, the transition dipole of the Tb is random, irrespective of the orientation of the complex itself.

Advantages and Limitations of Tb. Three important advantages afforded by the initial Tb donor have been demonstrated. First, with a sufficient lag-time, the time-gated emission observed is exclusively the product of energy transfer from the Tb and along the FRET cascade down the photonic wire. In contrast, the prompt dye emission includes both FRET-sensitized and directly excited contributions, such that the prompt measurements will reflect a heterogeneous distribution of FRET cascades initiated at different points along the wire. Although judicious selection of excitation wavelength will change the magnitude of the directly excited emission from each dye, the small Stokes shifts of most dyes, their spectral widths, and the required spectral overlap for efficient FRET will generally preclude exclusive excitation of the initial donor dye in the photonic wire. Although a nonissue for light harvesting applications, direct excitation of multiple dyes is a potential complicating factor for studies of FRET in multidimensional networks and structures, and for biophotonic logic and diagnostic applications. Time-gating avoids these complications. Second, time-gating minimizes the emission signals from fluorescent dyes that are not part of the photonic wire structure. Whereas prompt measurements of emission are overwhelmed by fluorescence from excess dyes, time-gated measurements largely avoid this problem because only dyes in proximity to Tb can sustain emission after the lag time has passed. This feature may be advantageous if assembling complex three-dimensional DNA structures that have modest assembly efficiencies or, more generally, under dilute conditions, where excess strands may help drive nanostructure formation. A third and similar advantage is that background emission from the sample matrix itself can be rejected by time-gating, as demonstrated here by mixing the photonic wires with serum. This capability is highly advantageous for applications in real biological samples because FRET cascades spanning the visible spectrum are typically initiated with blue or violet excitation light, which generates more intense background from sample matrices than longer excitation wavelengths (which afford fewer energy transfer steps). Tb-initiated FRET cascades thus have great promise for prospective biophotonic logic, diagnostic, and imaging applications.

Although the advantages afforded by the initial Tb donor are of great value, there are trade-offs associated with its use. The molar absorption coefficient of the Tb is relatively modest compared to many fluorescent dyes and quantum dots, limiting the overall brightness of the photonic wire, albeit compensated by the high quantum yield of the Tb and an improved signal-to-background ratio with time-gated measurements. The multiple emission lines of the Tb permit pairing with many possible dye acceptors but necessitate another level of spectral decomposition to analyze the dye emission, although greatly facilitated by their narrow spectral width. Finally, and similar to previous reports,[51] there is some evidence that Tb can nonspecifically associate with some fluorescent dyes. As shown in the SI, some limited time-gated emission from all of the dye-labeled DNA strands was observed when mixed with the free Tb complex at sufficiently high concentration (Figure S7A) and also when free dye was mixed with free Tb (Figure S7B). Such interactions

DOI: 10.1021/acsphotonics.5b00052
ACS Photonics 2015, 2, 639–652

may be responsible for (i) the anomalously high levels of time-gated A647 emission and Tb quenching in the Tb/A488-initiated photonic wire in Figure 5A and Figure 7, and (ii) the small increases in time-gated A488 and A594 emission in Figure 7B when an 8-fold excess of the corresponding segment strand is added to the template. The precise nature of these putative interactions is beyond our scope here, but may be driven, at least in part, by the mutual hydrophobicity of the Tb and fluorescent dyes. The extent of nonspecific association appears to vary with the selection of fluorescent dyes and their accessibility within a DNA nanostructure. For example, the Tb/A546-initiated photonic wire does not show anomalously high levels of emission from the A647 at an internal position (cf., the anomalously high emission when at a terminal position in the Tb/A488-initiated wire). These interactions can likely be avoided by working at submicromolar concentrations with carefully selected dyes. Overall, these few drawbacks are quite minor and would be far outweighed by the significant benefits afforded by the Tb and time-gated measurements.

CONCLUSIONS

We have demonstrated that a luminescent terbium complex (Tb) can be used to initiate a time-gated FRET cascade along a DNA/LNA photonic wire. The inclusion of the LNA nucleotides increased the thermal stability of the photonic wire structure, and the millisecond-scale emission lifetime of the Tb and its multiple, narrow emission lines provided several additional advantages. The long lifetime permitted time-gated measurements that minimized unwanted background emission from directly excited fluorescent dyes, whether from noninitial positions in the photonic wire or from excess strands. Time-gating also permitted rejection of background from biological sample matrices, and the multiple emission lines permitted initial energy transfer steps to a variety of fluorescent dyes across the visible spectrum. Moreover, observed efficiencies for Tb-to-dye energy transfer were closer to the predicted values than dye-to-dye energy transfer, which are postulated to be a consequence of the unpolarized emission of the Tb resulting in more favorable dipole orientation factors. The key to using the Tb as an effective initial donor was to position the next-in-line acceptor dye in a so-called "sweet spot." When the Tb and its next-in-line acceptor dye were too closely spaced, the high FRET efficiency decreased the Tb donor lifetime to an extent that Tb-sensitized emission shifted into the lag or delay time required for time-gated measurements. Conversely, too far a spacing between the Tb and its acceptor dye resulted in low energy transfer efficiencies and low levels of FRET-sensitized time-gated emission. Optimization of the spacing permitted time-gated emission measurements with high signal-to-background ratios. Overall, initiation of a time-gated FRET cascade with a Tb donor is a very promising strategy for the fundamental design and characterization of photonic wires and other functional DNA nanostructures, because it can improve signal-to-background in several ways, as demonstrated here along with the important design consideration of the "sweet spot."

ASSOCIATED CONTENT

Supporting Information

Table of DNA sequences, boxcar method for measuring emission lifetimes, method of calculation of FRET parameters, values for spectral overlap integrals, representative time-gated emission and excitation spectra for photonic wire permutations, data showing the effect of LNA on thermal stability, model for time-gated emission, and additional discussion on energy transfer processes. This material is available free of charge via the Internet at http://pubs.acs.org.

AUTHOR INFORMATION

Corresponding Author

*E-mail: algar@chem.ubc.ca.

Notes

The authors declare no competing financial interest.

ACKNOWLEDGMENTS

The authors acknowledge support from the Office of Naval Research (ONR). M.G.A. and I.L.M. acknowledge support from NRL and the NRL NSI. W.R.A. acknowledges support from the Canada Foundation for Innovation (CFI), a Canada Research Chair (Tier 2), and Michael Smith Foundation for Health Research Scholar Award. The authors thank Lumiphore, Inc. for the Lumi4-Tb-NHS reagent.

REFERENCES

(1) Garcia-Parajo, M. F.; Hernando, J.; Mosteiro, G. S.; Hoogenboom, J. P.; van Dijk, E.; van Hulst, N. F. Energy Transfer in Single-Molecule Photonic Wires. *ChemPhysChem* **2005**, *6*, 819–827.

(2) Pinheiro, A. V.; Han, D. R.; Shih, W. M.; Yan, H. Challenges and Opportunities for Structural DNA Nanotechnology. *Nat. Nanotechnol.* **2011**, *6*, 763–772.

(3) Teo, Y. N.; Kool, E. T. DNA-Multichromophore Systems. *Chem. Rev.* **2012**, *112*, 4221–4245.

(4) Tinnefeld, P.; Heilemann, M.; Sauer, M. Design of Molecular Photonic Wires Based on Multistep Electronic Excitation Transfer. *ChemPhysChem* **2005**, *6*, 217–222.

(5) Su, W.; Bonnard, V.; Burley, G. A. DNA-Templated Photonic Arrays and Assemblies: Design Principles and Future Opportunities. *Chem.—Eur. J.* **2011**, *17*, 7982–7991.

(6) Nangreave, J.; Han, D. R.; Liu, Y.; Yan, H. DNA Origami: A History and Current Perspective. *Curr. Opin. Chem. Biol.* **2010**, *14*, 608–615.

(7) Rothemund, P. W. K.; Andersen, E. S. Nanotechnology: The Importance of Being Modular. *Nature* **2012**, *485*, 584–585.

(8) Seeman, N. C. DNA Nanotechnology: Novel DNA Constructions. *Annu. Rev. Biophys. Biomol. Struct.* **1998**, *27*, 225–248.

(9) Seeman, N. C. Nanomaterials Based on DNA. *Annu. Rev. Biochem.* **2010**, *79*, 65–87.

(10) Kuzuya, A.; Komiyama, M. DNA Origami: Fold, Stick, and Beyond. *Nanoscale* **2010**, *2*, 310–322.

(11) Tan, L. H.; Xing, H.; Lu, Y. DNA as a Powerful Tool for Morphology Control, Spatial Positioning, and Dynamic Assembly of Nanoparticles. *Acc. Chem. Res.* **2014**, *47*, 1881–1890.

(12) Kuzuya, A.; Ohya, Y. DNA Nanostrutures as Scaffolds for Metal Nanoparticles. *Polymer J.* **2012**, *44*, 452–460.

(13) Matczyszyn, K.; Olesiak-Banska, J., DNA as Scaffolding for Nanophotonic Structures. *J. Nanophotonics* **2012**, *6*.

(14) Yu, X.; Lei, D. Y.; Amin, F.; Hartmann, R.; Acuna, G. P.; Guerrero-Martinez, A.; Maier, S. A.; Tinnefeld, P.; Carregal-Romero, S.; Parak, W. J. Distance Control In-Between Plasmonic Nanoparticles via Biological and Polymeric Spacers. *Nano Today* **2013**, *8*, 480–493.

(15) Buckhout-White, S.; Spillmann, C. M.; Algar, W. R.; Khachatrian, A.; Melinger, J. S.; Goldman, E. R.; Ancona, M. G.; Medintz, I. L. Assembling Programmable FRET Based Photonic Networks Using Designer DNA Scaffolds. *Nat. Commun.* **2014**, *5*, 5615.

(16) LaBoda, C.; Duschl, H.; Dwyer, C. L. DNA-Enabled Integrated Molecular Systems for Computation and Sensing. *Acc. Chem. Res.* **2014**, *47*, 1816–1824.

DOI: 10.1021/acsphotonics.5b00052
ACS Photonics 2015, 2, 639–652

(17) Jester, S. S.; Famulok, M. Mechanically Interlocked DNA Nanostructures for Functional Devices. *Acc. Chem. Res.* **2014**, *47*, 1700−1709.
(18) Kuzuya, A.; Ohya, Y. Nanomechanical Molecular Devices made of DNA Origami. *Acc. Chem. Res.* **2014**, *47*, 1742−1749.
(19) Rangnekar, A.; LaBean, T. H. Building DNA Nanostructures for Molecular Computation, Templated Assembly, and Biological Applications. *Acc. Chem. Res.* **2014**, *47*, 1778−1788.
(20) Tsukanov, R.; Tomov, T. E.; Liber, M.; Berger, Y.; Nir, E. Developing DNA Nanotechnology Using Single-Molecule Fluorescence. *Acc. Chem. Res.* **2014**, *47*, 1789−1798.
(21) Wang, Z. G.; Ding, B. Q. Engineering DNA Self-Assemblies as Templates for Functional Nanostructures. *Acc. Chem. Res.* **2014**, *47*, 1654−1662.
(22) Yang, D. Y.; Hartman, M. R.; Derrien, T. L.; Hamada, S.; An, D.; Yancey, K. G.; Cheng, R.; Ma, M. L.; Luo, D. DNA Materials: Bridging Nanotechnology and Biotechnology. *Acc. Chem. Res.* **2014**, *47*, 1902−1911.
(23) Sacca, B.; Niemeyer, C. M. DNA Origami: The Art of Folding DNA. *Angew. Chem., Int. Ed.* **2012**, *51*, 58−66.
(24) Albinsson, B.; Hannestad, J. K.; Borjesson, K. Functionalized DNA Nanostructures for Light Harvesting and Charge Separation. *Coord. Chem. Rev.* **2012**, *256*, 2399−2413.
(25) Kawahara, S.; Uchimaru, T.; Murata, S. Sequential Multistep Energy Transfer: Enhancement of Efficiency of Long-Range Fluorescence Resonance Energy Transfers. *Chem. Commun.* **1999**, 563−564.
(26) Ohya, Y.; Yabuki, K.; Hashimoto, M.; Nakajima, A.; Ouchi, T. Multistep Fluorescence Resonance Energy Transfer in Sequential Chromophore Array Constructed on Oligo-DNA Assemblies. *Bioconjugate Chem.* **2003**, *14*, 1057−1066.
(27) Heilemann, M.; Kasper, R.; Tinnefeld, P.; Sauer, M. Dissecting and Reducing the Heterogeneity of Excited-State Energy Transport in DNA-Based Photonic Wires. *J. Am. Chem. Soc.* **2006**, *128*, 16864−16875.
(28) Heilemann, M.; Tinnefeld, P.; Mosteiro, G. S.; Garcia-Parajo, M.; Van Hulst, N. F.; Sauer, M. Multistep Energy Transfer in Single Molecular Photonic Wires. *J. Am. Chem. Soc.* **2004**, *126*, 6514−6515.
(29) Spillmann, C. M.; Buckhout-White, S.; Oh, E.; Goldman, E. R.; Ancona, M. G.; Medintz, I. L. Extending FRET Cascades on Linear DNA Photonic Wires. *Chem. Commun.* **2014**, *50*, 7246−7249.
(30) Graugnard, E.; Kellis, D. L.; Bui, H.; Barnes, S.; Kuang, W.; Lee, J.; Hughes, W. L.; Knowlton, W. B.; Yurke, B. DNA-Controlled Excitonic Switches. *Nano Lett.* **2012**, *12*, 2117−2122.
(31) Sanchez-Mosteiro, G.; van Dijk, E.; Hernando, J.; Heilemann, M.; Tinnefeld, P.; Sauer, M.; Koberlin, F.; Patting, M.; Wahl, M.; Erdmann, R.; van Hulst, N. F.; Garcia-Parajo, M. F. DNA-Based Molecular Wires: Multiple Emission Pathways of Individual Constructs. *J. Phys. Chem. B* **2006**, *110*, 26349−26353.
(32) Boeneman, K.; Prasuhn, D. E.; Blanco-Canosa, J. B.; Dawson, P. E.; Melinger, J. S.; Ancona, M.; Stewart, M. H.; Susumu, K.; Huston, A.; Medintz, I. L. Self-Assembled Quantum Dot-Sensitized Multivalent DNA Photonic Wires. *J. Am. Chem. Soc.* **2010**, *132*, 18177−18190.
(33) Spillmann, C. M.; Ancona, M. G.; Buckhout-White, S.; Algar, W. R.; Stewart, M. H.; Susumu, K.; Huston, A. L.; Goldman, E. R.; Medintz, I. L. Achieving Effective Terminal Exciton Delivery in Quantum Dot Antenna-Sensitized Multistep DNA Photonic Wires. *ACS Nano* **2013**, *7*, 7101−7118.
(34) Algar, W. R.; Kim, H.; Medintz, I. L.; Hildebrandt, N. Emerging Non-Traditional Förster Resonance Energy Transfer Configurations with Semiconductor Quantum Dots: Investigations and Applications. *Coord. Chem. Rev.* **2014**, *263*−*264*, 65−85.
(35) Selvin, P. R.; Rana, T. M.; Hearst, J. E. Luminescence Resonance Energy Transfer. *J. Am. Chem. Soc.* **1994**, *116*, 6029−6030.
(36) Armelao, L.; Quici, S.; Barigelletti, F.; Accorsi, G.; Bottaro, G.; Cavazzini, M.; Tondello, E. Design of Luminescent Lanthanide Complexes: From Molecules to Highly Efficient Photo-Emitting Materials. *Coord. Chem. Rev.* **2010**, *254*, 487−505.
(37) Hildebrandt, N.; Wegner, K. D.; Algar, W. R. Luminescent Terbium Complexes: Superior Förster Resonance Energy Transfer Donors for Flexible and Sensitive Multiplexed Biosensing. *Coord. Chem. Rev.* **2014**, *273*−*274*, 125−138.
(38) Bunzli, J. C. G. Lanthanide Luminescent Bioprobes (LLBs). *Chem. Lett.* **2009**, *38*, 104−109.
(39) Marriott, G.; Heidecker, M.; Diamandis, E. P.; Yanmarriott, Y. Time-Resolved Delayed Luminescence Image Microscopy Using an Europium Ion Chelate Complex. *Biophys. J.* **1994**, *67*, 957−965.
(40) Hemmila, I.; Laitala, V. Progress in Lanthanides as Luminescent Probes. *J. Fluoresc.* **2005**, *15*, 529−542.
(41) Hagan, A. K.; Zuchner, T. Lanthanide-Based Time-Resolved Luminescence Immunoassays. *Anal. Bioanal. Chem.* **2011**, *400*, 2847−2864.
(42) Geißler, D.; Charbonnière, L. J.; Ziessel, R. F.; Butlin, N. G.; Löhmannsröben, H. G.; Hildebrandt, N. Quantum Dot Biosensors for Ultra-Sensitive Multiplexed Diagnostics. *Angew. Chem., Int. Ed.* **2010**, *49*, 1396−1401.
(43) Geißler, D.; Stufler, S.; Löhmannsröben, H. G.; Hildebrandt, N. Six-Color Time-Resolved Förster Resonance Energy Transfer for Ultrasensitive Multiplexed Biosensing. *J. Am. Chem. Soc.* **2013**, *135*, 1102−1109.
(44) Xu, J.; Corneillie, T. M.; Moore, E. G.; Law, G. L.; Butlin, N. G.; Raymond, K. N. Octadentate Cages of Tb(III) 2-Hydroxyisophthalamides: A New Standard for Luminescent Lanthanide Labels. *J. Am. Chem. Soc.* **2011**, *133*, 19900−19910.
(45) James, D. R.; Siemiarczuk, A.; Ware, W. R. Stroboscopic Optical Boxcar Technique for Determination of Fluorescence Lifetimes. *Rev. Sci. Instrum.* **1992**, *63*, 1710−1716.
(46) Lakowicz, J. R. *Principles of Fluorescence Spectroscopy*, 3rd ed.; Springer Science+Business Media: New York, 2007.
(47) Algar, W. R.; Wegner, D.; Huston, A. L.; Blanco-Canosa, J. B.; Stewart, M. H.; Armstrong, A.; Dawson, P. E.; Hildebrandt, N.; Medintz, I. L. Quantum Dots as Simultaneous Acceptors and Donors in Time-Gated Förster Resonance Energy Transfer Relays: Characterization and Biosensing. *J. Am. Chem. Soc.* **2012**, *134*, 1876−1891.
(48) Cywiński, P. J.; Hammann, T.; Hühn, D.; Parak, W. J.; Hildebrandt, N.; Löhmannsröben, H. G. Eurpoium-Quantum Dot Nanobioconjugates as Luminescent Probes for Time-Gated Biosensing. *J. Biomed. Opt.* **2014**, *19*, 101506.
(49) Wegner, K. D.; Morgner, F.; Oh, E.; Goswami, R.; Susumu, K.; Stewart, M. H.; Medintz, I. L.; Hildebrandt, N. Three-Dimensional Solution-Phase Förster Resonance Energy Transfer Analysis of Nanomolar Quantum Dot Bioconjugates with Subnanometer Resolution. *Chem. Mater.* **2014**, *26*, 4299−4312.
(50) Wegner, K. D.; Lanh, P. T.; Jennings, T.; Oh, E.; Jain, V.; Fairclough, S. M.; Smith, J. M.; Giovanelli, E.; Lequeux, N.; Pons, T.; Hildebrandt, N. Influence of Luminescence Quantum Yield, Surface Coating, and Functionalization of Quantum Dots on the Sensitivity of Time-Resolved FRET Bioassays. *ACS Appl. Mater. Interfaces* **2013**, *5*, 2881−2892.
(51) Algar, W. R.; Malanoski, A. P.; Susumu, K.; Stewart, M. H.; Hildebrandt, N.; Medintz, I. L. Multiplexed Tracking of Protease Activity Using a Single Color of Quantum Dot Vector and a Time-Gated Förster Resonance Energy Transfer Relay. *Anal. Chem.* **2012**, *84*, 10136−10146.
(52) Petersen, M.; Wengel, J. LNA: A Versatile Tool for Therapeutics and Genomics. *Trends Biotechnol.* **2003**, *21*, 74−81.
(53) Karkare, S.; Bhatnagar, D. Promising Nucleic Acid Analogs and Mimics: Characteristic Features and Applications of PNA, LNA, and Morpholino. *Appl. Microbiol. Biotechnol.* **2006**, *71*, 575−586.
(54) Briones, C.; Moreno, M. Applications of Peptide Nucleic Acids (PNAs) and Locked Nucleic Acids (LNAs) in Biosensor Development. *Anal. Bioanal. Chem.* **2012**, *402*, 3071−3089.
(55) Wang, L.; Yang, C. J.; Medley, C. D.; Benner, S. A.; Tan, W. Locked Nucleic Acid Molecular Beacons. *J. Am. Chem. Soc.* **2005**, *127*, 15664−15665.

DOI: 10.1021/acsphotonics.5b00052
ACS Photonics 2015, 2, 639−652

(56) Wengel, J. Synthesis of 3′-C- and 4′-C-Branched Oligodeoxynucleotides and the Development of Locked Nucleic Acid (LNA). *Acc. Chem. Res.* **1999**, *32*, 301−310.
(57) Mikheikin, A. L.; Zhuze, A. L.; Zasedatelev, A. S. Binding of Symmetrical Cyanine Dyes into the DNA Minor Groove. *J. Biomol. Struct. Dyn.* **2000**, *18*, 58−72.

DOI: 10.1021/acsphotonics.5b00052
ACS Photonics 2015, 2, 639−652